Hindawi Publishing Corporation
International Journal of Rotating Machinery
Volume 2007, Article ID 85275, 10 pages
doi:10.1155/2007/85275

Research Article

Optimization Design and Experimental Study of Low-Pressure Axial Fan with Forward-Skewed Blades

Li Yang, Ouyang Hua, and Du Zhao-Hui

School of Mechanical Engineering, Shanghai Jiaotong University, Shanghai 200030, China

Received 8 February 2007; Accepted 9 July 2007

Recommended by Y. Ohta

This paper presents an experimental study of the optimization of blade skew in low pressure axial fan. Using back propagation (BP) neural network and genetic algorithm (GA), the optimization was performed for a radial blade. An optimized blade is obtained through blade forward skew. Measurement of the two blades was carried out in aerodynamic and aeroacoustic performance. Compared to the radial blade, the optimized blade demonstrated improvements in efficiency, total pressure ratio, stable operating range, and aerodynamic noise. Detailed flow measurement was performed in outlet flow field for investigating the responsible flow mechanisms. The optimized blade can cause a spanwise redistribution of flow toward the blade midspan and reduce tip loading. This results in reduced significantly total pressure loss near hub and shroud endwall region, despite the slight increase of total pressure loss at midspan. In addition, the measured spectrums show that the broadband noise of the impeller is dominant.

1. INTRODUCTION

Skewed and swept blade technique was originated from the research achievements of aircraft airfoil. Since this technique was introduced to turbomachinery field, it has played a very important role in the performance improvement of turbomachinery. So far, many research results have proved that the skewed and/or swept technique would promote aerodynamic efficiency, reduce throughflow losses, enhance stable range, as well as decrease the aerodynamic noise of turbomachinery.

Beiler and Carolus [1] studied the aerodynamic performance of both forward- and backward-swept impellers of the low-speed axial fans. The results showed that the forward-swept blades could improve the aerodynamic performance and have the potential of widespread application. However, there was poor performance in aerodynamics of the backward-swept blades. Cai et al. [2] presented an experimental investigation and numerical simulation of the performance of an axial-flow fan with skewed rotating blades. The results showed that the performance of the forward-skewed blade increased at a higher pressure rise of 13.1% and gave a larger flow rate of about 5%, as well as a higher efficiency of more than 3% and a lower noise of 2 to 4 dBA. Outa [3] studied rotating stall performance of a single stage subsonic axial compressor and found that forward-swept blade would increase throttle margin with decreased tip loss. Corsini and Rispoli [4] proved that the forward-swept blade of a subsonic axial fan operates more efficiently in particular at low flow rates, with a delayed onset of stall.

With the development of computer technology and optimization algorithms, optimum design of turbomachinery with swept and skewed blade to be concerned has become practicable.

One notable attempt to study the optimization of blade in transonic axial compressor was achieved by Yi et al. [5, 6]. The optimal impeller with backward-swept and skewed blades is designed based on simulated annealing (SA) methods. Experimental results showed that the adiabatic efficiency of the optimal impeller is increased by 0.82%, while the flow rate and total pressure ratio were kept constant. Besides, further efficiency promotion of 1.05% was also achieved by using Gradient Method (GM), with the optimum parameters of swept angle and blade camber curves. Jang et al. [7, 8] designed a backward-swept impeller in transonic axial compressor by using response surface method (RSM). The adiabatic efficiency of optimum impeller was increased by 1.25%. The separation line, which was defined as interference between shock and boundary layer of blade suction surface, was moved to further downstream of the optimal impeller.

With concern to the optimization of skewed and swept blades in low-pressure axial fan, Yu and Yuan [9] introduced

an optimization procedure of a multistage axial compressor with inlet guide vane (IGV) and outlet guide vane (OGV) by using design of experiment (DOE) and sequential quadratic programming (SQP). Main optimization parameter is the swept and skewed blade stacking line. The efficiency of the optimized impeller was increased by 1.26%, the mass flow rate was increased by 1.56%, total pressure ratio was increased by 1.77%, as well as the surge margin that was extended by 9.38%. Lotfi et al. [10, 11] also showed the optimization of blade camber line of low-speed axial fan by using GA method would achieve higher efficiency than the original design. In our former work [12], aerodynamic and aeroacoustic performances of radial, forward-skewed, and backward-skewed blades of low pressure axial fan have been studied contrastively. Both skewed angle of forward and backward impeller is set as 8.3 deg. It is shown that the forward-skewed impeller has a noise reduction of 4.3 dBA and the stable operating range extended by 5.69%, compared to the radial impeller. However, the aerodynamic efficiency and total pressure rise is decreased by 3.53% and 5.63%, respectively.

In present study, optimization design of skewed angle is carried out based on former impeller parameters described in [12]. An optimization algorithm based on GA and BP neural network is adopted in present work, as well as three-dimensional (3D) Reynolds-averaged Navier-Stokes (RANS) computational fluid dynamics (CFD) simulation to determine the aerodynamic performance during the optimization procedure. The performance promotion of optimized impeller is confirmed by experiment, and the flow mechanism is also explained by detailed flow field measurements.

2. SKEWED BLADE AND STUDY MODEL

2.1. Skewed blade

So far, there is not a unified definition of skewed blade in turbomachinery field. In this paper, circumferential-skewed blade is defined as follows. Figure 1 illustrates the stacking line ABC of blade which is observed from the axial direction of the impeller. The stacking line is composed of straight line segment and arc segment. The straight line segment is AB and the arc segment is BC. Point "A" is located on the hub and point "C" is located at the blade tip. Point "B" is the intersection of the arc and the straight-line of the stacking line. Point "O" is located on the axis of the impeller. As shown in the figure, the angle δ_{sk} between line OB and line OC is called circumferential skewed angle of the blade. If the angle δ_{sk} is more than 0°, it shows that the skewed direction of the blade is along rotation direction of the impeller and vice versa. They are called the circumferential forward-skewed blade and the circumferential backward-skewed blade, respectively.

2.2. Study model

In this case, the optimization of blade skew is based on a blade of a kind of low-pressure axial flow fan. Table 1 summarizes the key design parameters. As shown in Table 1, because the circumferential-skewed angle of the archetypal blade is very small, it can be approximately regarded as radial blade. More detailed descriptions of the impeller are described in [12].

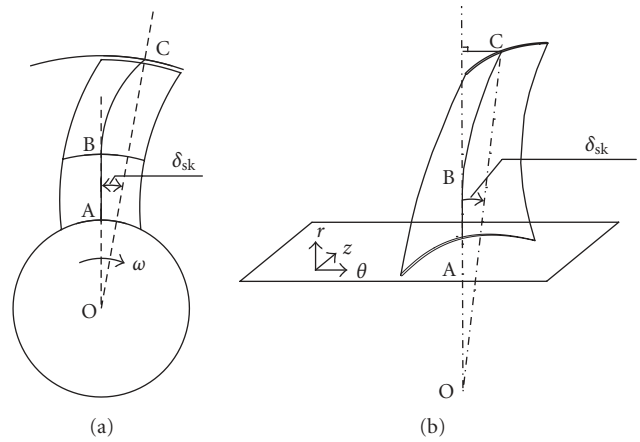

Figure 1: Schematic of stacking line of blade.

Table 1: Key design parameters of archetypal impeller.

Impeller speed n (r· min^{-1})	1440
Tip radius r_t (m)	0.2475
Hub-tip ratio ν	0.35
Number of blade Z	5
Blade stagger angle β (deg)	25
Tip clearance ε_R/r_t	1.5%
Circumferential-skewed angle of blade δ_{sk} (deg)	1.27

3. OPTIMIZATION DESIGN

Optimization design system consists of a parameterized blade geometry description, 3D RANS flow solver, and an optimization procedure, as shown in Figure 2. The parameterized blade geometry is generated by the geometry program (GEOM). The commercial European aerodynamic numerical simulator (EURANUS) [13] is selected as 3D RANS flow solver. The optimization tool includes GA and artificial neural network (ANN) with BP training.

At first, the blade geometry is defined by a few number of design parameters in GEOM. A database with multiple samples is created and the CFD results of each sample are stored in the database with 3D RANS flow solver. With the widely adopted BP learning algorithm and the trained ANN, an optimization model constructing the relationship between the input variables (blade geometry variables) and output variables (i.e., efficiency, total pressure ratio) is setup. At last, the final results of the optimization parameters are achieved based on GA and 3D RANS flow solver.

3.1. Parameterization of blade geometry

The parametric blade representation includes the parametric blade sections, at different spanwise locations, the location

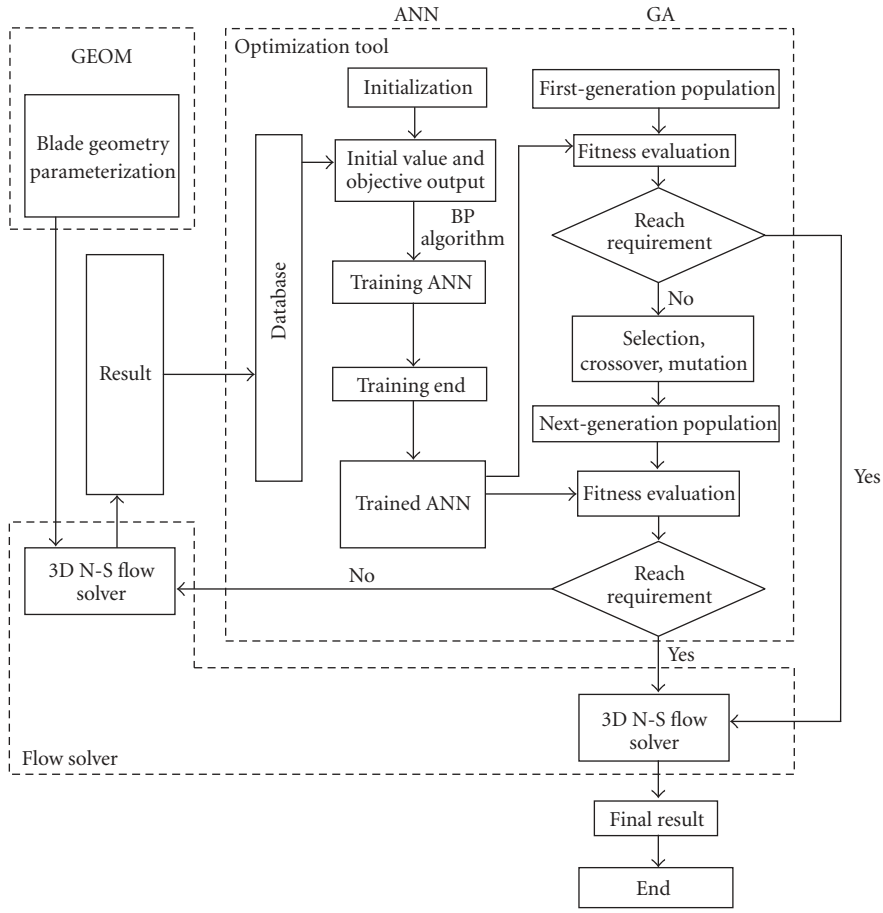

Figure 2: Optimization design system.

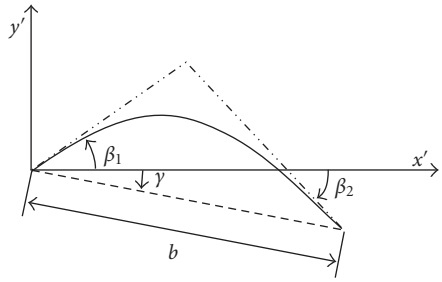

Figure 3: Blade camber curve definition.

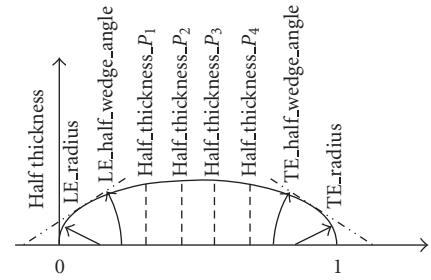

Figure 4: 2D-blade profile definition.

of the stacking point on the blade sections, and the parametric stacking line of the blade. The whole 3D-blade geometry of the impeller is combined of eight blade sections in the spanwise direction, which are located at $\lambda = 0, 0.25, 0.38, 0.5, 0.63, 0.75, 0.87$, and 1.00, respectively. In the parametric blade sections, a simple second-order Bezier curve is used to define the camber curve (Figure 3). Both the pressure side and the suction side curve of the 2D-blade profiles are defined by third-order Bezier curve. There are the rounded leading edge (LE) and trailing edge (TE) of the 2D-blade profiles (Figure 4). The stacking points are located in the center of gravity of 2D-blade section. In the circumferential direction, the stacking line is controlled by a composite curve, including a third-order Bezier curve, a straight-line and a third-order Bezier curve (Figure 5).

As shown in Figure 5, α_1 is the angle of the first Bezier curve at span = 0. Parameter C_1 is the spanwise extent of the first Bezier curve. Parameter P_1 is the fractional factor defining the second control point location of the first Bezier curve. α_2 is the angle of the linear segment, and α_3 is the angle of the second Bezier curve at span = 1. Parameter C_2 is the spanwise extent of the second Bezier curve. Parameter P_2 is the fractional factor defining the second control point location of the second Bezier curve.

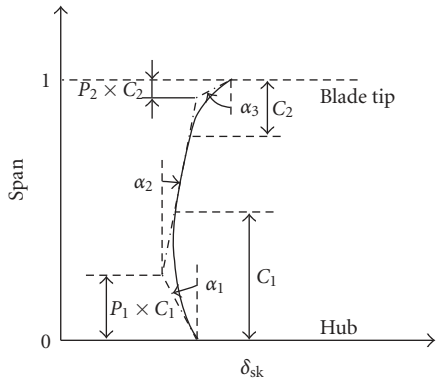

Figure 5: 3D stacking line definition.

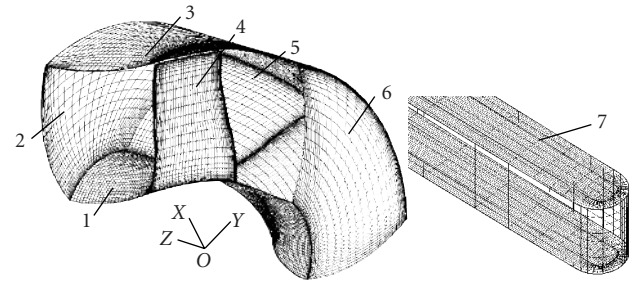

1. Hub
2. Outlet
3. Shroud
4. Blade
5. Periodic boundary
6. Inlet
7. Tip clearance

Figure 6: Computational mesh.

3.2. Numerical method

The three-dimensional, incompressible, viscous flow is computed with the EURANUS. In this optimization, the simulator solves the Reynolds-averaged form of Navier-Stokes equations.

The turbulence is modeled by Spalart-Allmaras (S-A) [14] one-equation turbulence model for this application. The spatial discretization is based on a finite-volume approach allowing a fully conservative discretization based on a central formulation. A time discretization is applied through a fourth order Runge-Kutta procedure. An efficient combination of multigrid and implicit residual averaging is used for convergence acceleration to steady state, which is helpful to shorten time of optimization design.

A structured mesh, generated by using the interactive grid generator (IGG) [15], is required in the optimization computation of the archetypal blade. The computation mesh consists of three blocks. One block is in the passage and the others are at the tip clearance (Figure 6). Generally, a small alteration of blade geometry shape can have more negative impact on I-mesh quality than on H-mesh quality. This may result in the increase of "bad" samples in the database with I-mesh. Therefore, the H-mesh is only used in the flow passage, in present optimization. In the flow passage, the mesh contains 129 points in the streamwise direction, 73 points in the spanwise direction, and 65 points in the azimuthal direction. The mesh in the tip clearance is embedded into the H&O-mesh. A tip clearance block with O-mesh contains 13 points in the spanwise direction, 13 points in the azimuthaldirection, and 161 points wrapping around the tip of the blade. The other tip clearance block with H-mesh contains 13 points in the spanwise direction, 17 points in the azimuthal direction, and 65 points in the streamwise direction.

The boundary conditions are defined as follows. The inlet flow condition is specified from measured total pressure, total temperature, and flow angle from axial direction. The outlet flow condition is specified from mass flow rate and static pressure. In the S-A turbulence model, turbulence viscosity at inlet is given. The boundary conditions specified at the hub and the blades are rotating walls in the fixed reference frame. The shroud is a stationary wall in the fixed reference frame. The periodic boundary condition is imposed for the upstream and downstream of the blade, and inside the tip clearance.

In the computation, the convergence criteria are as follows.

(1) The mass flow balance error should be lower than 5×10^{-5}.
(2) The variations of the global quantities (efficiency, pressure ratio, etc.) should remain lower than 5×10^{-3}.
(3) The maximum of all normalized residues is less than 1×10^{-4}.

3.3. Optimization algorithm

This optimization tool is an algorithm based on BP neural network and GA. GA, based on the evolution theories of Darwin and the genetics of Mendel, is a global optimization algorithm. A population of individuals changes over a number of generations using the mechanisms of selection, crossover, and mutation, whereby the best individual is always transferred unchanged to the next generation. ANN, based on the process of imitating brain to solve problem, is an intelligent information processing technology. By some network topology, many basic processing elements (neuron models) are connected to be a neural network. Using ANN, some information processing functions are carried out. The processing functions are similar to the brain to learn, recognize, and remember and so forth.

The algorithm has highly efficient global optimization ability of GA and strong local searching and learning of ANN. The optimization design systems with only GA or ANN have been examined, however none are found to be better than the algorithm in optimization time and accuracy of predicted results.

3.4. Objective function

The two of parameters controlling the blade stacking line in circumferential direction are chosen to be design variables in this optimization. The two design variables are angle α_2 and α_3 (Figure 5) and the other parameters are invariable during this optimization. This means that straigh-line "AB" is

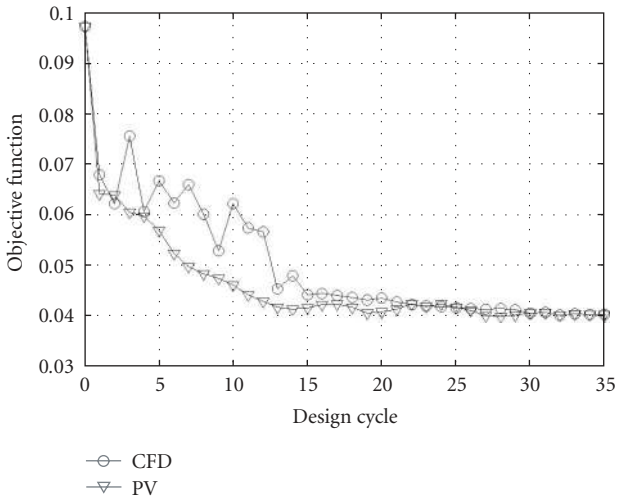

Figure 7: Evolution curve of objective function.

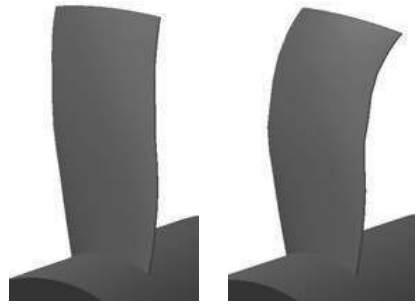

(a) Archetypal blade (b) Optimized blade

Figure 8: 3D models of archetypal blade and optimized blade.

invariable and the shape of arc "BC" may be altered in this optimization. Point "B" is located at $\lambda = 0.4$ (Figure 1). An initial database with 20 samples is created. In each sample, the two design variables are chosen randomly between the given lower and upper bounds. According to experience and experimental results obtained from former designs, the variation ranges of the two design variables are from $-30°$ to $30°$. Thus, 20 blades with different circumferential-skewed angles are obtained. The computational mesh of each sample is generated and the internal flow field is simulated.

In this optimization, the objective function is to maximize efficiency and total pressure rise (equation (1)). At the same time, constraints are imposed on the mass flow rate (equation (2)),

$$f(X) = m_1 \cdot (1-\eta)^k + m_2 \cdot \left(\frac{P_{\text{imp}} - P_c}{P_{\text{ref}}}\right)^k, \quad (1)$$

$$(1-M)G_1 \le G_2 \le (1+M)G_1. \quad (2)$$

Imposed value of total pressure P_{imp} is usually more than true value. The two pressures P_{ref} and P_{imp} are set to equality. The weight factors m_1 and m_2 show the influences of efficiency and total pressure rise in the objective function, respectively. Both the weight factors are set to 1.0. Exponent factor k is set to 2.0. Constraint factor M is set to 0.5%.

Figure 7 presents the evolution curve of the objective function in this optimization. Curve "PV" is prediction values by BP neural network and GA. Curve "CFD" is a computation result of the samples by 3D N-S flow solver. As shown in the figure, with the increase of the iteration numbers, the value of the objective function is less and less. Near the 30th step, the value of the objective function shows little variation. It indicates that the result converges and the optimal result is finally achieved.

3.5. Optimization result

The optimization result shows that the circumferential-skewed angle of the optimized blade is 6.1 deg. Figure 8 presents the 3D models of the archetypal blade and the optimized blade. As shown in Figure 8, the optimized blade is a typical circumferential forward-skewed blade.

4. EXPERIMENTAL SETUP

In order to evaluate the performance, both aerodynamic and aeroacoustic experiments have been carried out in the anechoic chamber of the turbomachinery laboratory of Shanghai Jiaotong University. The aerodynamic performance test follows GB/T 1236-2000 standard [16] and the aeroacoustic performance test follows GB/T 2888-91 standard [17]. The designed fan test rig consists of test impeller, driving unit, experimental appliances, and duct system (Figure 9).

The test impellers include the archetypal impeller and the optimized impeller. The impeller is connected directly to an electromotor YSF-8014. Using a frequency converter Sanken MF-7.5K-380, the rotary speed of the motor is controlled. The rotary speed is obtained by a noncontact photoelectric digital tachometer SZG-441C. As shown in Figure 9, the performance parameters of the test impellers are obtained with the experimental appliances, including the manometer for static pressure, the pitot probe for total pressure, the sound level meter for overall sound pressure level, and so on. Using the throttle cone, which has a diameter of 600 mm, the flow rate of the fan is changed. In addition, the cone can prevent environment noise from entering the anechoic chamber by the duct system. Hence, it is also very helpful to reduce the error of aeroacoustic measurement.

Measurement of outlet flow field is performed with five-hole probe. The measured points are located on the plane AB (Figure 9), which is at 15 mm behind the outlet of the impeller. On the plane, the aerodynamic parameters of 21 points along radial direction of the blade are measured. More detailed descriptions of the experimental design and measurement methods are given in [12].

5. RESULTS AND DISCUSSION

5.1. Aerodynamic performance

Figure 10 shows the aerodynamic performance comparison between archetypal impeller and the optimized impeller with

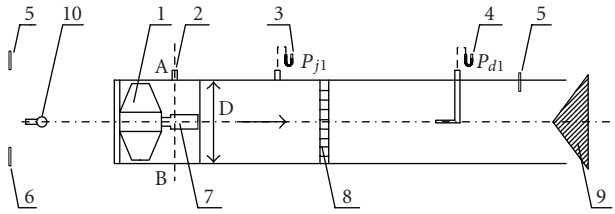

1. Test impeller
2. Five-hole probe
3. Manometer
4. Pitot probe
5. Thermometer
6. Barometer
7. Electromotor
8. Streamlined lattice
9. Throttle cone
10. Sound-level meter

Figure 9: Experimental setup.

Table 2: Comparison of aerodynamic performance between two impellers at design condition.

	Archetypal impeller	Optimized impeller
ψ	0.0675	0.0699
$\eta(\%)$	76.25	77.52

forward-skewed blades. Key dimensionless aerodynamic parameters are defined as follows:

$$\varphi = \frac{Q}{\pi U_t r_t^2},$$
$$\psi = \frac{P_t}{\rho U_t^2}, \tag{3}$$
$$\Delta = \frac{Q_1 - Q_{\min}}{Q_{\min}}.$$

Both the total pressure rise and efficiency of optimized impeller are higher than archetypal impeller at almost all flow rate range, except $\varphi = 0.20 \sim 0.22$. At the design flow rate condition $\varphi = 0.245$, the total pressure efficiency of the optimized impeller is increased by 1.27% and its total pressure rise is increased by 3.56%, as compared to the archetypal impeller. Detailed results are shown in Table 2. As described in Section 1, the efficiency and total pressure rise of forward-skewed impeller with skewed angle of 8.3 deg is decreased of 3.53% and 5.63%, compared to the archetype radial impeller. This obvious difference proves that the optimization design method is effective in skewed blade design. At off-design low flow rate conditions, as shown in Figure 10(a), the minimum stable volume flow coefficient of the optimized impeller is significantly extended from 0.2 to 0.18, which stands for a wider stable operation range for present axial fan.

5.2. Aeroacoustic performance

Figure 11 shows the overall sound pressure level (SPL) and the average A-weight sound pressure level of the two impellers at various flow rates. The average A-weight sound pressure level is defined as overall A-weight sound pressure level of unit flow rate and unit total pressure, which is more effective to evaluate fan noise with different flow rate and total pressure rise. The definition of average A-weight sound pressure level is

$$L_{SA} = L_A - 10\lg\left(QP_t^2\right) + 19.82. \tag{4}$$

As shown in Figure 11, the SPL will increase at low flow rate range, and decrease at stable operation flow range. The minimum SPL of stable flow range is located at design flow rate condition $\varphi = 0.245$, where the overall sound pressure level L_A and the average A-weight sound pressure level L_{SA} of the optimized impeller are decreased by 6.5 dBA compared to archetypal impeller.

Figure 12 shows the one third octave spectrum of the two impellers at the design condition. As shown in Figure 12, noise frequency domain of the two impellers is from 100 Hz to 10 000 Hz. It indicates that the broadband noise is dominant in the measured spectrums. In the whole frequency domain, the SPL of the optimized impeller is lower compared to the archetypal impeller. In the frequency domain of [300 Hz, 4000 Hz], the difference between the two impellers in the SPL is more obvious than in the other domain. It indicates that the frequency domain between 300 Hz and 4000 Hz is the chief part of noise reduction in the optimized impeller.

5.3. Detailed flow field

In order to measure the detailed flow field and figure out the difference between archetypal and optimized impeller, five-hole aerodynamic probe is adopted in present study to carry out outlet flow field measurement of these two impellers. Figure 13 illustrates the spanwise distribution of circumferentially averaged total pressure loss coefficient at the outlet of the two impellers at the design condition. The total pressure loss coefficient is defined as

$$C_{pt} = \frac{\left(p_{1w}^* - p_{2w}^*\right)}{(1/2)\rho W_1^2}. \tag{5}$$

As shown in Figure 13, the spanwise distribution of total pressure loss coefficient reveals that most of the aerodynamic losses are converged to the near wall regions, namely, blade tip ($\lambda > 0.7$) and hub ($\lambda < 0.1$). The losses of the main flow region ($0.1 < \lambda < 0.7$) are relatively lower. Furthermore, the C_{pt} of the optimized impeller is obviously decreased at both blade tip and hub region, as well as increased at mid-span. According to the radial-equilibrium equation, since line "BC" of the stacking line is skewed obviously along rotation direction of the impeller (Figure 1), the radial component of the body force, which is in reverse radial direction, is increased obviously. As a result, low-energy fluid accumulation near the shroud endwall moves to the mid-span region and the loss near the shroud endwall is deceased. In the lower mid-span region, the stacking line shape is unchanged and the centrifugal force is still predominant. Hence, low energy fluid accumulation near the hub endwall still moves to the mid-span region. The experimental results show that in the optimized impeller, the decrease of the blade tip loss is 2.2 times more than the increase of the loss in the mid-span region. It indicates that the circumferential skew of the

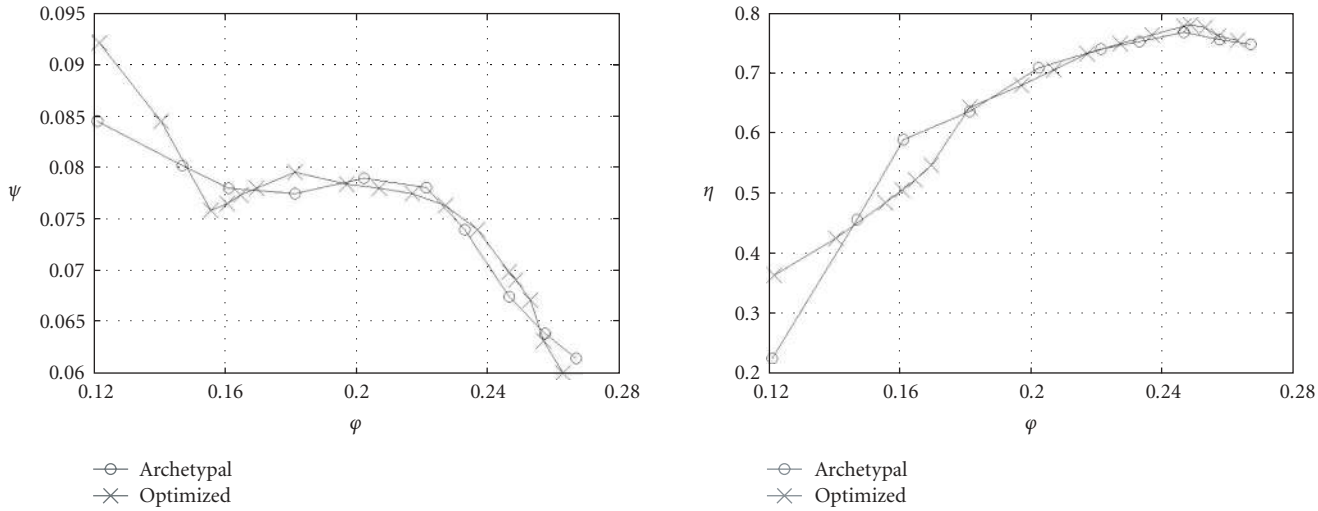

(a) Total pressure coefficient

(b) Total pressure efficiency

Figure 10: Aerodynamic performance curves.

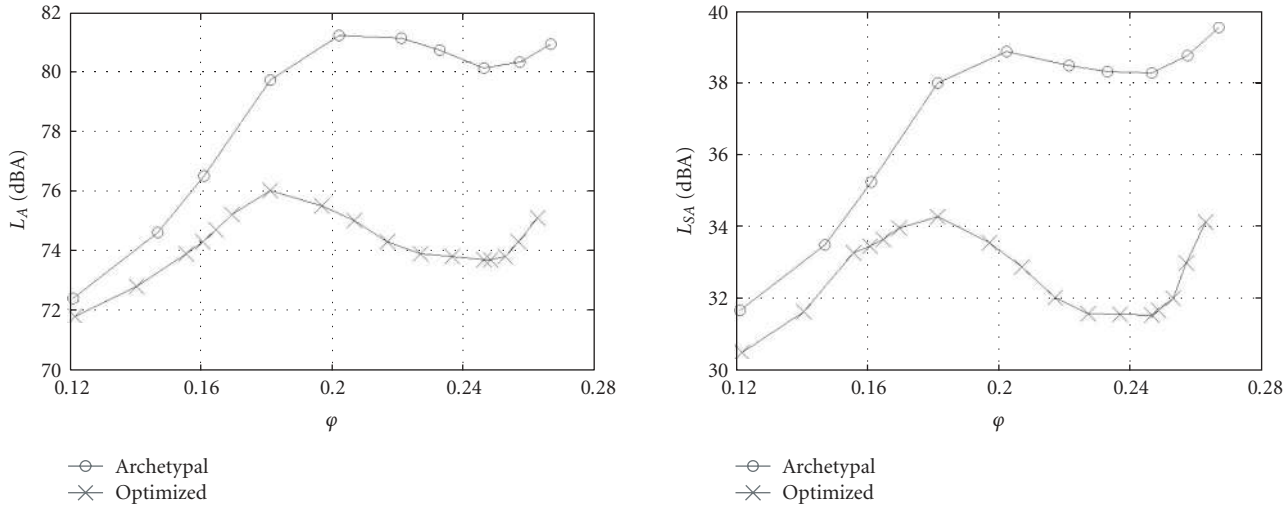

(a) Overall sound pressure level

(b) Average A-weight sound pressure level

Figure 11: Aerodynamic performance curves.

blade may have beneficial impact on the spanwise redistribution of the total pressure loss. The blade with the appropriate circumferential-skewed angle can reduce the loss in the flow field and increase aerodynamic efficiency of the fan.

Figure 14 presents the spanwise distribution of circumferentially averaged total pressure rise at the outlet of the two impellers at the design condition. The maximum of total pressure rise at the outlet of the archetypal impeller is in the upper mid-span region, which is $0.8 < \lambda < 0.9$. The maximum of total pressure rise at the outlet of the optimized impeller is near the mid-span region, which is $0.5 < \lambda < 0.7$. According to the radial-equilibrium equation, spanwise pressure distribution is determined by the centrifugal force in the archetypal impeller, which results in the increase of blade loading of the upper mid-span. However, the radial component of the body force generated by skewed blade is opposite to the centrifugal force. As a result, the impact of the centrifugal force is weakened in the upper mid-span region. In the lower mid-span region, the main forces (i.e., centrifugal force) are unchanged. It results in the increase of the blade loading of the mid-span in the optimized impeller. The experimental results indicate that, in the optimized impeller, the increase of the total pressure rise in the region of $0.2 < \lambda < 0.8$, is 1.4 times higher than the decrease of the blade tip total pressure rise.

Figures 15 and 16 show the spanwise distribution of circumferentially averaged axial velocity and the computed distribution of axial velocity at the outlet of the two impellers

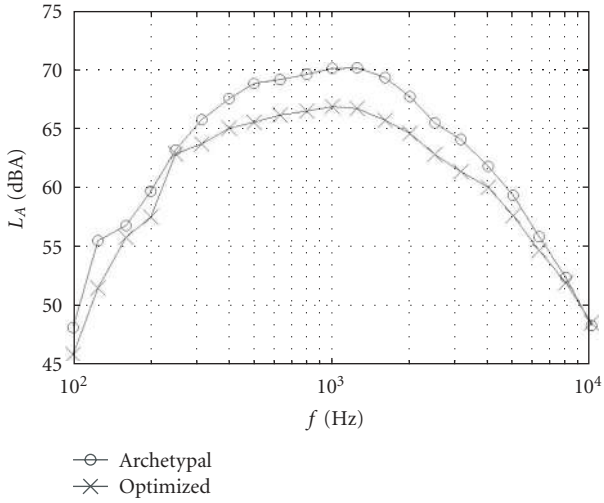

Figure 12: one-third octave spectrum.

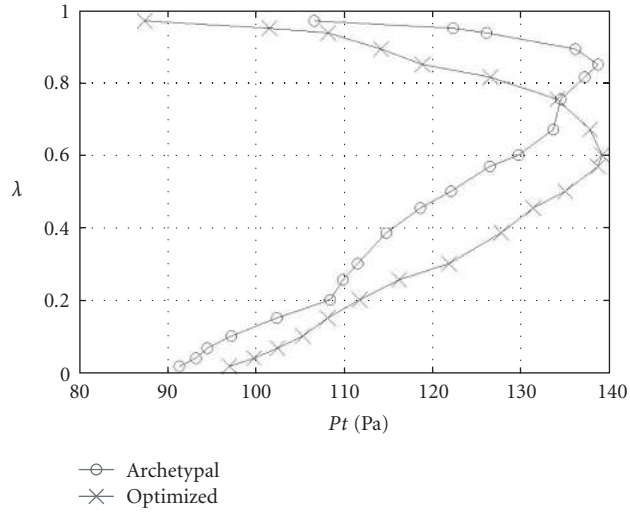

Figure 14: Spanwise distribution of total pressure rise.

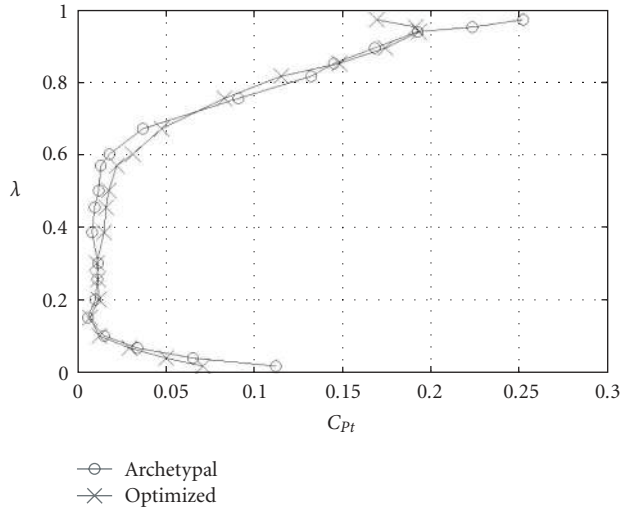

Figure 13: Spanwise distribution of total pressure loss coefficient.

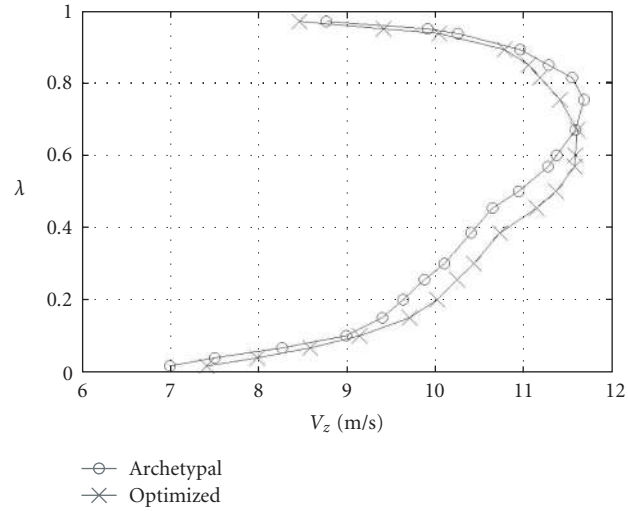

Figure 15: Spanwise distribution of axial velocity.

at the design condition, respectively. As shown in Figure 15, the distribution of axial velocity is similar to the distribution of total pressure rise in the two impellers. The maximum of flow rate at the outlet of the archetypal impeller is in the upper mid-span region, which is $0.7 < \lambda < 0.8$. The maximum of flow rate at the outlet of the optimized impeller is near the mid-span region, which is $0.5 < \lambda < 0.7$. It shows that the circumferential skew of the blade has great impact on the spanwise redistribution of flow rate. In addition, there is obviously improved flow in the corner zone between suction surface of blade and shroud in the optimized impeller (Figure 16). It has a beneficial impact on the delay of onset of stall and the extension of stable operating range.

6. CONCLUSIONS

(1) The aerodynamic optimization design of forward-skewed blade of low-pressure axial flow fan has been achieved by BP neural network and GA optimization method. Both aerodynamic and aeroacoustic performances of optimized impeller with forward-skewed angle of 6.1 deg have been improved with comparison to the archetype radial impeller. The total pressure efficiency is increased by 1.27%, total pressure rise is increased by 3.56%. The stable operating range of the optimized impeller is greatly extended to more than 30%, as well as aerodynamic noise reduced by more than 6 dB(A) at design operating condition. In addition, detailed spectrums indicate that the broadband noise of the impeller is dominant. The optimization design procedure has been proved to be effective to further skewed and swept impeller design.

(2) Detailed flow field results indicate that the impeller with forward-skewed blades would cause a spanwise redistribution of flow rate and pressure toward the blade midspan, as well as reduce tip loading. The aerodynamic losses of optimized impeller are decreased significantly near blade

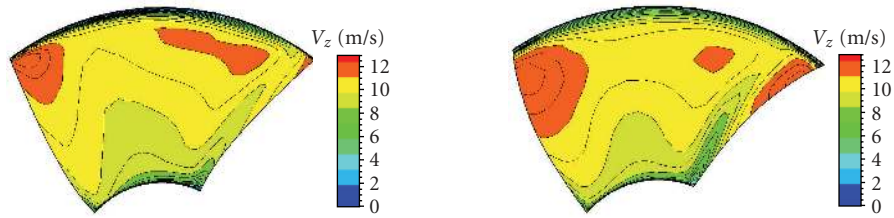

(a) Archetypal impeller (b) Optimized impeller

Figure 16: Distribution of axial velocity.

shroud and hub endwall region with only few penalty of mid-span. The overall pressure losses are obviously lower than the archetype radial impeller, which results in higher efficiency and lower noise.

NOMENCLATURE

r: Radial (m)
θ: Circumferential (deg)
z: Axial (m)
r_h: Hub radius
r_t: Tip radius
n: Impeller speed ($\mathrm{r}\cdot \mathrm{min}^{-i}$)
v: Hub-tip ratio = r_h/r_t
Z: Number of blade
λ: Blade span = r/r_t
β: Blade stagger angle (deg)
ε_R: Tip clearance (m)
ρ: Fluid density (Kg/m^3)
P_{imp}: Imposed value of total pressure (Pa)
P_{ref}: Reference value of total pressure (Pa)
P_c: Computational value of total pressure (Pa)
m_1, m_2: Weight factor of objective function
k: Exponent factor of objective function
G_1: Initial value of mass flow rate (Kg/s)
G_2: Final value of mass flow rate (Kg/s)
M: Constraint factor of mass flow rate
U_t: Tangential velocity of blade tip (m/s)
Q: Volume flow rate (m^3/s)
P_t: Total pressure rise (Pa)
N: Shaft power (W)
φ: Flow rate coefficient
Ψ: Total pressure coefficient
η: Total pressure efficiency
Q_{min}: Minimum flow rate before flow separation (m^3/s)
Q_1: Flow rate at peak efficiency point (m^3/s)
Δ: Stable operating range
L_A: Overall sound pressure level (dBA)
L_{SA}: Average A-weight sound pressure level
W: Relative velocity (m/s)
p^*_{1w}: Inlet Stagnation pressure (Pa)
p^*_{2w}: Outlet Stagnation pressure (Pa)
C_{Pt}: Total pressure loss coefficient

REFERENCES

[1] M. G. Beiler and T. H. Carolus, "Computation and measurement of the flow in axial flow fans with skewed blades," *Journal of Turbomachinery*, vol. 121, no. 1, pp. 59–66, 1999.

[2] N. Cai, J. Xu, and A. Benaissa, "Aerodynamic and aeroacoustic performance of a skewed rotor," in *Proceedings of ASME Turbo Expo, International Gas Turbine Institute Conference (IGTI '03)*, vol. 6A, pp. 497–504, Atlanta, Ga, USA, June 2003.

[3] E. Outa, "Rotating stall and stall-controlled performance of a single stage subsonic axial compressor," *Journal of Thermal Science*, vol. 15, no. 1, pp. 1–13, 2006.

[4] A. Corsini and F. Rispoli, "The role of forward sweep in subsonic axial fan rotor aerodynamics at design and off-design operating conditions," in *Proceedings of ASME Turbo Expo, International Gas Turbine Institute Conference (IGTI '03)*, vol. 6A, pp. 543–553, Atlanta, Ga, USA, June 2003.

[5] W.-L. Yi, H.-Y. Huang, and W.-J. Han, "Optimized design of axial compressor blades," *Journal of Engineering for Thermal Energy and Power*, vol. 21, no. 2, pp. 140–144, 2006 (Chinese).

[6] W.-L. Yi, H.-Y. Huang, and W.-J. Han, "Application of a simulated annealing and response surface model in optimization design of moving compressor vanes," *Power Engineering*, vol. 26, no. 4, pp. 483–485, 524, 2006 (Chinese).

[7] C.-M. Jang, P. Li, and K.-Y. Kim, "Optimization of blade sweep in a transonic axial compressor rotor," *JSME International Journal, Series B: Fluids and Thermal Engineering*, vol. 48, no. 4, pp. 793–801, 2006.

[8] C.-M. Jang, A. Samad, and K.-Y. Kim, "Optimal design of swept, leaned and skewed blades in a transonic axial compressor," in *Proceedings of the 51st ASME Turbo Expo*, vol. 6B, pp. 1279–1288, Barcelona, Spain, May 2006.

[9] H. Yu and X. Yuan, "Optimized aerodynamic design of multiblade rows of an axial compressor," *Journal of Engineering for Thermal Energy and Power*, vol. 20, no. 6, pp. 603–606, 2005 (Chinese).

[10] O. Lotfi, J. A. Teixeira, P. C. Ivey, G. Sheard, and I. R. Kinghorn, "Aerodynamic optimization of industrial fan blade cascades," in *Proceedings of the ASME Turbo Expo—Gas Turbie Technology*, vol. 6B, pp. 1059–1066, Reno-Tahoe, Nev, USA, June 2005.

[11] O. Lotfi, J. A. Teixeira, P. C. Ivey, I. R. Kinghorn, and A. G. Sheard, "Shape optimisation of axial fan blades using genetic algorithms and a 3D Navier-Stokes solver," in *Proceedings of*

the 51st ASME Turbo Expo, vol. 6B, pp. 1373–1383, Barcelona, Spain, May 2006.

[12] H. Ouyang, Y. Li, Z.-H. Du, and F.-Y. Zhong, "Experimental study on aerodynamic and aero-acoustic performance of low pressure axial flow fan with circumferential skewed blades," *Journal of Aerospace Power*, vol. 21, no. 4, pp. 668–674, 2006 (Chinese).

[13] *FINE^{TM} Numeca's Flow Integrated Environment*, NUMECA International, Brussels, Belgium, User Manual, Version 6.2, 2004.

[14] P. R. Spalart and S. R. Allmaras, "One-equation turbulence model for aerodynamic flows," *Recherche Aerospatiale*, no. 1, pp. 5–21, 1994.

[15] *IGG^{TM} Highly Interactive Geometry Modeler and Grid Generator*, NUMECA International, Brussels, Belgium, User Manual, version 4.9-1, 2004.

[16] *Test Methods of Aerodynamic Performance for Fans*, Standards Press of China, Beijing, China, 2000.

[17] *Methods of Noise Measurement for Fans, Blower Compressors and Roots Blowers*, Standards Press of China, Beijing, China, 1991.